Growth, spectroscopic, and laser properties of Yb^{3+}-doped $Lu_3Al_5O_{12}$ garnet crystal

A. Brenier, Y. Guyot, H. Canibano, and G. Boulon

Laboratoire de Physico-Chimie des Matériaux Luminescents, CNRS Unité Mixte de Recherche (UMR 5620), Université Claude Bernard-Lyon1, 10 Rue Ampère, 69622 Villeurbanne, France

A. Ródenas and D. Jaque

Grupo de Espectroscopía Láser, Departamento de Fìsica de Materiales, Universidad Autònoma de Madrid, Cantoblanco Universidad, Madrid 28049, Spain

A. Eganyan and A. G. Petrosyan

Laboratory for Crystal Growth of Luminescent Materials, Institute for Physical Research, 378410 Ashtarak-2, Armenia

Received March 23, 2005; revised July 22, 2005; accepted September 7, 2005; posted October 28, 2005 (Doc. ID 61099)

We have grown high-quality LuAG:Yb^{3+} crystals with 0.75, 3.8, 10, 12, 15, 20, and 50 at. % concentrations by the vertical Bridgman method. With low-temperature spectroscopy the Stark sublevel structure of the $^2F_{7/2}$ ground state and the $^2F_{5/2}$ excited state has been determined. With room-temperature spectroscopy, the emission cross section was found to be 3×10^{-20} cm^2, being 1.5 times the YAG:Yb^{3+} emission cross section. The luminescence quantum efficiency was measured in samples with different Yb^{3+} concentrations. Its value was found to be 90% for 3.8 and 10 at. %, 84% for 20 at. %, and 70% for 50 at. % Yb^{3+}. The laser-emission tunability under diode pumping was found to extend from 1045 up to 1095 nm in a 12 at. % sample with 3.15 mm thickness.

OCIS codes: 140.3380, 140.3480, 140.0140.

1. INTRODUCTION

The first lasing LuAG:Yb^{3+} crystal was reported in mid-1970's under Xe lamp pumping. This laser operated at 77 K with an output wavelength of 1.0294 μm and with a typical laser threshold of 1 J.[1] Then lasing was demonstrated under 970 nm laser-diode pumping,[2] and a thorough study of the temperature dependence of the laser efficiency was performed.[3] Nowadays, the pump sources are high-power InGaAs laser diodes emitting around 980 nm. Their advantage is to reduce the quantum defect and then the thermal loading of the crystal during laser operation. High-power cw applications are possible, all the more so that no upconversion or excited-state absorption losses can occur with Yb^{3+}, contrary to Nd^{3+}.

$Lu_3Al_5O_{12}$ (LuAG) belongs to the rare-earth garnet family (space group O_h^{10}-$Ia3d$) with lattice spacing 11.906 Å,[4] 11.907–11.923 Å.[5] The linear thermal-expansion coefficient of LuAG is (8.8 ± 0.3) 10^{-6} (290–1275 K), and the refractive index is 1.8424 ($\lambda=0.589$ μm).[6] Another interesting property of garnets for lasing is their good thermal conductivity: 10.7 $W\,m^{-1}\,K^{-1}$ for $Y_3Al_5O_{12}$(YAG), 8 $W\,m^{-1}\,K^{-1}$ for $Gd_3Ga_5O_{12}$(GGG),[7] and 8 $W\,m^{-1}\,K^{-1}$ for LuAG.[8]

In the majority of cases, oxide laser crystals are grown by melt techniques, including the vertical Bridgman method.[9] There are minimal chemical heterogeneities in crystals grown by this method, mainly owing to low temperature gradients that can be attained in this geometry and absence of rotation; furthermore, this method provides for the possibility to grow several crystals in one run, which is important to obtain concentration series under similar growth conditions. The melting point of LuAG is 2060 C; the hardness (Moh's value) is 8.5.

This paper is devoted to the growth of LuAG:Yb^{3+} single crystal by the vertical Bridgman method and to the study of its room- and low-temperature spectroscopic properties, including the measurements of the luminescence quantum yield. Lasing properties, including thermal loading and laser tunability, are also studied under the end-diode pumping configuration at 970 nm.

2. CRYSTAL GROWTH AND CHARACTERIZATION

LuAG:Yb^{3+} single crystals were grown by the vertical Bridgman method using 99.99% pure starting oxides of Lu_2O_3, Yb_2O_3, and Al_2O_3, and molybdenum crucibles. To eliminate second-phase precipitation and to provide for single-phase garnet crystals, the melt compositions were selected with account of octahedral site occupancy by small rare-earth ions.[5] Single crystals of LuAG:Yb were grown from melts with Yb concentrations equal to 0.71, 3.8, 10, 12, 15, 20, and 50 at.% with respect to Lu. To suppress the faceting effect and to provide for high-quality material, most of the crystals were grown along the ⟨001⟩ direction using seed crystals cut from undoped LuAG. The

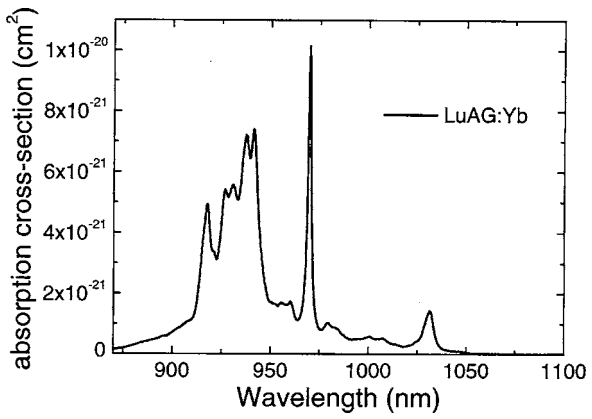

Fig. 1. Room-temperature absorption spectrum of LuAG:Yb^{3+}.

typical boule size was 15 mm in diameter and 60 mm in length. Owing to a small size difference between Yb and Lu ions, the distribution coefficient of Yb in LuAG is close to unity, so the concentration of Yb in the melt and the crystal is about the same. The rare-earth ions normally fill the dodecahedral lattice sites, but a small amount of Lu and Yb may also enter the octahedral lattice sites; distribution of the rare earth over different crystallographic sites can be represented as $\{Lu_{3-x}Yb_x\}\times[Al_{2-y-z}Lu_yYb_z]Al_3O_{12}$, where the z value increases with the Yb/Lu ratio in the melt, while the $(y+z)$ value is between 0.01 and 0.05. Estimations based on site occupancy data[5] give the following values for the octahedral concentration of Yb: ~0.25% in LuAG:Yb (50%) and ~0.001% in LuAG:Yb (10%). At such low concentrations, the octahedral-coordinated Yb may reveal itself in absorption or emission spectra only as weak satellite lines, which however have not been identified in the studied crystals.

The color of as-grown LuAG:Yb crystals was green-to-blue (depending on crystal composition) owing to two wide absorption bands in the visible range, which are associated with Yb^{2+} centers stable at 300 K;[10] the tail of the longer-wavelength absorption band extends to 1 μm and may introduce optical losses. Occurrence of Yb^{2+} states is favored by slightly reducing the atmosphere under which the crystal growth has been processed. To remove the color by stimulating $Yb^{2+}\rightarrow Yb^{3+}$ valence transitions, the obtained crystals were annealed at 1200 C in air. Discoloration occurring because of an exchange of oxygen between the surrounding gaseous environment and the crystal could be traced as a function of time by the movement of the boundary separating the crystal portions with different oxidation states of ytterbium, i.e., Yb^{3+}; and Yb^{3+} plus Yb^{2+}. The time of annealing required for complete discoloration, which is dependent on the crystal size but also on the as-grown concentration of Yb^{2+}, was optimized to produce clear crystals with no residual absorption.

Optical methods were applied for the assessment of quality and the selection of crystal portions free of occasional defects, introducing light refraction or scattering, that were used for fabrication of elements of spectroscopic and laser quality.

3. SPECTROSCOPIC PROPERTIES

A. Spectroscopy

The absorption spectra of different Yb^{3+} concentration samples were recorded with a Perkin–Elmer spectrophotometer. The absorbance is linear with Yb content; only very small differences can be seen in the different spectra. The room-temperature absorption cross section is shown in Fig. 1. The main peak with 2 nm FWHM corresponds to the "zero line" at 969.6 nm, but high absorption exists also near 940 nm. These two wavelengths are convenient for laser-diode pumping. At this point it should be noted that the absorption cross section around 970 nm obtained with Yb:LuAG (1×10^{-20}) is higher than that corresponding to Yb:YAG (0.7×10^{-20}),[11] ensuring a more efficient pump absorption.

The emission spectrum $I(\lambda)$ was recorded with a nitrogen-cooled North Coast germanium cell under near infrared excitation at 940 nm, through a Raman shifter, with a Quantel Datachrome dye laser pumped with a frequency-doubled pulsed YAG:Nd Quantel laser. The room-temperature emission cross section σ_e is shown in Fig. 2. It was established with the formula

$$\sigma_e(\lambda)=\frac{\lambda^4 I(\lambda)}{8\pi c\,\tau_{\mathrm{rad}} n^2 \int I(\lambda)\mathrm{d}\lambda}, \tag{1}$$

where τ_{rad} is the radiative fluorescence lifetime equal to the fluorescence lifetime obtained from extrapolation at zero Yb content of the lifetimes of the different samples (see below, next paragraph). In practice we have chosen the lowest concentrated sample (1.01 ms for the 0.75% sample), as in this case self-trapping effects are minimized. In Eq. (1) $n=1.82$ is the LuAG refractive index of refraction. Interestingly, we have found that the σ_e peak value 3×10^{-20} cm^2 is higher than YAG:Yb^{3+}:2.03×10^{-20} cm^2,[3,11] meaning that LuAG:Yb is more suitable for short-pulse extraction.

The fluorescence lifetime was measured with a digital Lecroy oscilloscope for different Yb^{3+} concentrations under 10 ns pulsed excitation. It increased first with an increasing concentration owing to reabsorption of emitted light; this is the self-trapping effect,[12] which has also been

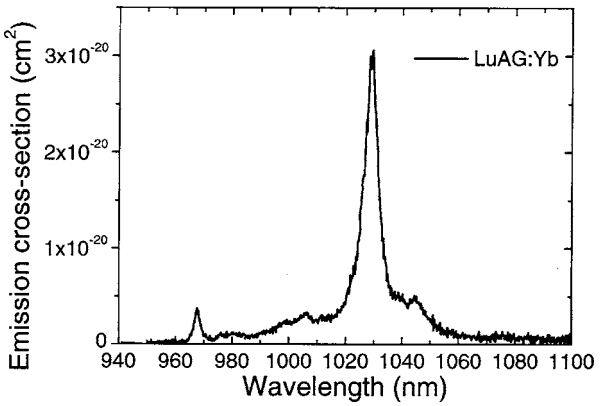

Fig. 2. Room-temperature emission spectrum of LuAG:Yb^{3+}.

Table 1. Fluorescence Lifetime versus Yb^{3+} Content in LuAG

Yb^{3+} Content (%)	0.75	3.8	10	15	20	50
Lifetime (ms)	1.01	1.169	1.317	0.83	0.525	0.208

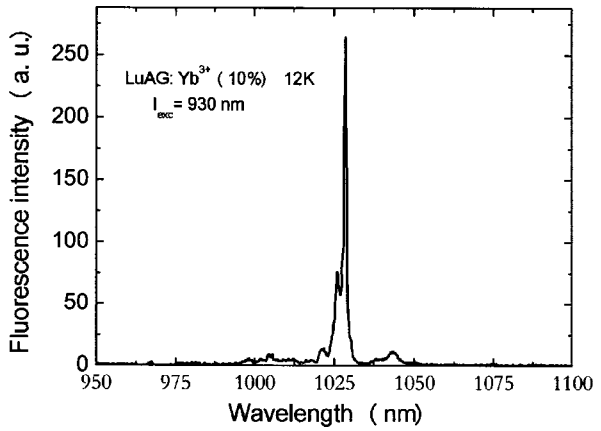

Fig. 3. Low-temperature emission spectrum of LuAG:Yb^{3+}.

observed in such other garnets as YAG:Yb^{3+}[13] and GGG:Yb^{3+}.[14,15] Then the lifetime decreased owing probably to nonradiative losses towards traps. The losses are quantitatively studied in Subsection 4.B. The measured lifetimes for different Yb^{3+} samples are gathered in Table 1.

Low-temperature absorption and emission spectra were recorded with samples located inside a liquid-helium flux cryostat; they are shown in Figs. 3 and 4. The room-temperature absorption at 969.6 nm is larger than that observed in the same wavelength at low temperature. We have no clear explanation for that; we can notice that these results do not agree with those reported in Ref. 3 for YAG:Yb but are in agreement with the GGG:Yb case.[14] Inspection of the different peaks and comparison with YAG:Yb^{3+}[13] Rand GGG:Yb^{3+}[14] Stark energy levels diagram lead to the sublevels energy positions in LuAG:Yb^{3+} gathered in Table 2.

B. Luminescence Quantum Efficiency

The fluorescence quantum efficiency (ϕ defined as the ratio of the number of radiative de-excitations to the total number of de-excitations from an energy state in a given laser system) is one of the most important parameters used to optimize the performance of a solid-state laser.[16] The heat delivered to the laser medium after the pumping process (optical or electric) is strongly determined by the value of the metastable state quantum efficiency. Crystals with low quantum efficiencies have higher nonradiative decay probabilities and show larger thermal loading rates than samples with high quantum efficiencies. This factor is of particular relevance for Yb^{3+} lasers, since these lasers operate in a quasi-three-level scheme so that pump power at threshold increases linearly with the nonvanishing population of the terminal laser level. This population increases continuously with the crystal temperature.[17] As the laser threshold depends strongly on the crystal temperature, the pump-to-laser conversion efficiency in diode-pumped Yb^{3+} lasers has been found to decrease drastically when the crystal temperature is increased.[18] The local temperature, the temperature in the pumping volume, is proportional to the fraction of pump power delivered to the crystal lattice as heat, and this fraction is determined by the particular value of the quantum efficiency of the metastable state.[19]

Up to now, the quantum efficiency of ion-doped crystals has been measured by photoacoustic and photothermal methods.[20,21] These methods provide good results but require relatively complicated experimental setups. An estimation of the quantum efficiency can be also obtained from the knowledge of both radiative (τ_R) and fluorescence (τ_F) lifetimes, which are related by the following expression:

$$\phi = \frac{\tau_F}{\tau_R}. \tag{2}$$

In rare-earth doped-laser crystals, the radiative lifetime is usually calculated by applying the so-called Judd–Ofelt formalism.[22] This method has provided excellent results when applied to Nd^{3+}-doped crystals, but it cannot be applied to the case of Yb^{3+}-doped crystals, because of the lack of absorption bands. For the particular case of Yb^{3+}-doped crystals, the radiative lifetime can be calculated from the analysis of absorption and emission cross sections.[20] Unfortunately, the knowledge of the actual value of fluorescence lifetime of Yb^{3+} ions is a complicated task, as time-decay curves of Yb^{3+} ions are usually affected by the self-absorption effect.[12] Thus alternative methods are required to obtain a direct and error-free measurement of Yb^{3+} quantum efficiency. In this work we will take advantage of a the multiwavelength photothermal method,[23] consisting of the measurement of the pump-induced crystal heating for different pump wavelengths, to determine the fluorescence quantum efficiency of Yb^{3+} ions in LuAG crystals as a function of ion concentration.

A schematic energy-level structure of Yb^{3+} ions in LuAG crystals is illustrated in Fig. 5, together with the relevant transitions involved in the quantum efficiency determination. After optical excitation from the ground state ($^2F_{7/2}$) to the excited state ($^2F_{5/2}$), a nonradiative relaxation takes place down to the emitting sub-Stark level

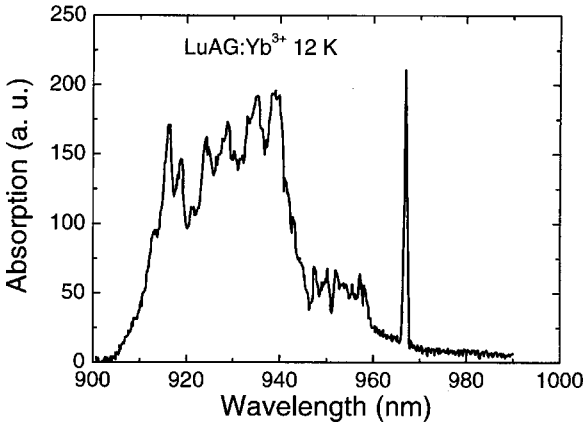

Fig. 4. Low-temperature absorption spectrum of LuAG:Yb^{3+}.

Table 2. Splitting of the Yb^{3+} Levels in Garnet Hosts

Host	$^2F_{7/2}$ Sublevel Energies (cm^{-1})	Barycenter (cm^{-1})	$^2F_{5/2}$ Sublevel Energies (cm^{-1})	Barycenter (cm^{-1})
LuAG	0 600 635 762	499	10330 10645 10900	10625
YAG	0 581 619 786	497	10327 10634 10927	10629
GGG	0 462 540 657	414	10309 10582 10811	10567

of the $^2F_{7/2}$ manifold Then, from the $^2F_{5/2}$ level, radiative and nonradiative transitions to the ground state, including transfers toward traps (not clearly identified at this step) take place with probabilities equal to ϕ and $1-\phi$, respectively. After the de-excitation, a final internal thermalization among the Stark sublevels of the ground state occurs. In the schematic diagram of Fig. 5 we have considered that all the radiative relaxations lead to the emission of a photon with a fixed wavelength equal to λ_F taken as the average fluorescence wavelength calculated from the room-temperature emission spectrum. In our particular case, we have obtained $\lambda_F \approx 1020$ nm; this value has been calculated from the room-temperature emission spectrum and has been found to be almost independent of the Yb^{3+} concentration. Following the excitation–de-excitation scheme of Fig. 5, the heat released to the sample comes from the internal relaxations at the upper and lower levels as well as from the nonradiative contribution. The steady value of the increase in crystal temperature, ΔT_{st}, which is proportional to the heat transferred to the sample, can be written as a function of pump wavelength as[23]

$$\Delta T_{st}\kappa N(\lambda_p)\left[\frac{10^7}{\lambda_p} - E_1 + \phi\left(E_1 - \frac{10^7}{\lambda_F}\right) + (1-\phi)E_1\right] = \kappa N(\lambda)\left[\frac{10^7}{\lambda_p} - \phi\frac{10^7}{\lambda_F}\right], \quad (3)$$

where $N(\lambda_p)$ is the number of excited ions per unit time, κ is a constant that depends on geometrical conditions and on the thermocouple–crystal contact, and λ_p is the excitation wavelength (in nanometer). The problem now is to calculate the number of excited ions per unit time for the different pump wavelengths used [$N(\lambda_p)$]. This number can be calculated by dividing the absorbed pump power by the energy of the pump photons.[23] Therefore we can state

$$N(\lambda_p) = \alpha P_{abs}(\lambda_P)\lambda_P, \quad (4)$$

where α is a constant independent on pump wavelength and $P_{abs}(\lambda_P)$ is the absorbed pump power. As we will see, the evaluation of the constant α is no longer necessary for the determination of quantum efficiency. Now, substituting Eq. (4) in Eq. (3) we obtain

$$\frac{\Delta T_{st}(\lambda_P)}{P_{abs}(\lambda_P)} = \alpha\kappa 10^7\left[1 - \phi\frac{\lambda_P}{\lambda_F}\right]. \quad (5)$$

Equation (5) indicates that if the ratio $[\Delta T_{st}(\lambda_P)]/[P_{abs}(\lambda_P)]$ is measured for different pump wavelengths, the value of the fluorescence quantum efficiency can be obtained by simply fiting the data to a linear relationship. Following this method we do not need any reference sample or any comparison with data obtained from the diluted samples. Additionally, the quantum efficiency for each particular sample has been calculated by comparing crystal thermal loading obtained under different pump wavelengths, so that we are only considering the change in the nonradiative decays caused by changes in the pumped level. In this way possible effects caused by self-trapping are minimized, and the values obtained for quantum efficiency can be considered, in a first-order approximation, quite close to the intrinsic values.

We have then performed this kind of measurement to determine the dependence of fluorescence quantum efficiency on the Yb^{3+} concentration in LuAG crystals. For this purpose, the Yb^{3+}:LuAG crystals were placed in a Teflon holder, and a cromel–alumel thermocouple was mechanically attached to the sample. The beam from a tunable (900–980 nm) argon-pumped Ti:sapphire laser was focused into the sample by a single 15 cm focal length lens. The pump beam followed a Gaussian distribution, and its waist diameter at the input crystal face was set to 2 mm. Pump power was kept equal to 700 mW for all the pump wavelengths used in this work. The voltage provided by the cromel–alumel thermocouple was measured by a digital nanovoltmeter. Temperature accuracy was below 1°C. The time employed for each temperature measurement was 3 min, this being quite larger than the time required for the sample to reach a steady temperature (typically below 1 min), and for each temperature measurement we wait close to 1 min. Additionally, a calibrated Si detector was placed behind the output crystal face, so that the pump power reaching this detector for each wavelength was recorded with and without the

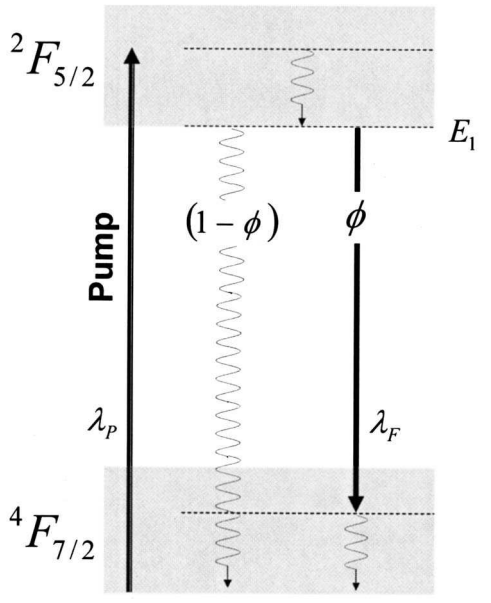

Fig. 5. Schematic energy-level structure of Yb^{3+} ions in LuAG. The relevant transitions involved in the quantum-efficiency determination are indicated by arrows.

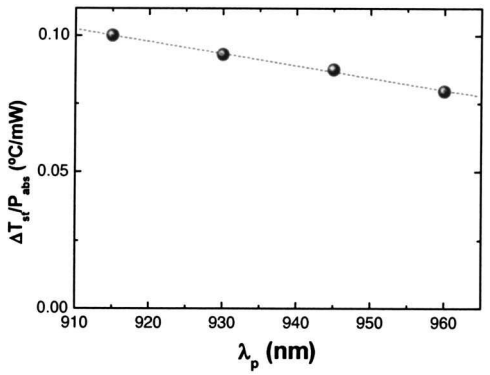

Fig. 6. Ratio between crystal-temperature increment and absorbed pump power as a function of pump wavelength obtained from the 3.8 at.% doped Yb^{3+}:LuAG sample.

Yb^{3+}:LuAG crystal. From these measurements the absorbed pump power for each wavelength was calculated. Finally, an additional thermocouple was used to measure the sample chamber in order to calculate the increase in crystal temperature. All the experiments carried out in this work were performed in a sample chamber with controlled temperature (±1°C). In addition, our experimental setup was placed within a laminar flux system in such a way that the thermal heating of the atmosphere surrounding the sample was avoided. As a consequence we can state that the temperature of the surrounding atmosphere was kept constant during experiments. Finally, it should be noted here that the measured crystal temperature was independent of the contact point between the crystal and the thermocouple with an accuracy of 5%.

Figure 6 shows a typical result obtained with our experimental setup. The date displayed in this figure corresponds to the 3.8 at.%-doped Yb^{3+}:LuAG sample. As can be appreciated, the $[\Delta T_{st}(\lambda_P)]/[P_{abs}(\lambda_P)]$ ratio decreases linearly as the pump wavelength increases, in accordance with Eq. (5). From the fit of the experimental data to a linear behavior, the dashed curve in Fig. 6, the fluorescence quantum efficiency can be obtained (in this case $\phi = 0.9 \pm 0.05$). We have carried out similar measurements for different Yb^{3+} concentrations. The corresponding values obtained for the fluorescence quantum efficiency are summarized in Fig. 7. As can be observed, quantum efficiency is close to one for relatively low concentrated samples (Yb^{3+} concentration below ≅10 at%). For higher concentrations the fluorescence quantum efficiency starts to decrease, indicating the activation of luminescence quenching probably related to energy migration among Yb^{3+} ions and the presence of luminescence killers. Such a behavior was also encountered in YAG:Yb^{3+}[11,13] but much less pronounced in Ref. 11.

4. LASER PROPERTIES

In this section the performance of Yb^{3+}-doped LuAG crystals as a laser gain medium under a cw diode pumping is studied. In Subsection 4.A we analyze the pump-induced thermal loading of a gain Yb^{3+}-doped LuAG laser crystal, and these measurements have been used for an alternative estimation of the fluorescence quantum efficiency. In Subsection 4.B we explore the possibility of tunable laser light generation around 1.06 μm from diode-pumped Yb^{3+}-doped LuAG crystals.

For the characterization of Yb^{3+}-doped LuAG crystals as a laser gain medium we have used a double-pass quasi-hemispherical cavity with a flat dichroic input mirror (IM; $R > 99.9\%$ at 1.06 μm and $T = 90\%$ at 980 nm). The output coupler (OC) was of 10 cm radius of curvature. Different OC transmittances (0.3 and 1%) were used. All of the OCs were also of high reflectance ($R > 90\%$) at the pump wavelength. End pumping was performed by a 50 μm fiber-coupled 2 W laser diode (Unique-ModeVDM38) emitting at 970 nm. The fiber output was first collimated and then focused by a single 3 cm focal lens into the crystal. The pumping mode radius (ω_P) was measured to be approximately 45 μm. The cavity length was 9.9 cm, leading to a laser beam waist ω_L of about 56 μm, so that $a = \omega_L/\omega_P \approx 1$, as is required for optimum pump and laser mode overlap.[17] The Yb^{3+}:LuAG crystal was placed as close as possible to input mirror. Among all the different Yb^{3+} concentrated crystals available in this work, optimum results were obtained for the 12 at.% doped sample and 3.15 mm thickness (the faces were not antireflection coated), so that all the results shown in this section correspond to this particular sample. The optimum performance obtained for the 12% doped sample adhers the fact that laser performance is enhanced because of the stronger pump absorption. If Yb^{3+} concentration is further increased, luminescence quenching takes place, leading to a strong thermal loading that is well known to deteriorate the laser performance of Yb^{3+} doped laser crystals. Lower-concentrated crystals suffer from lower thermal loading, but they show a poor pump absorption. At this concentration the fraction of absorbed pump power was high enough to ensure efficient absorption of pump radiation. Higher Yb^{3+} concentrations have led to deterioration in the observed laser performance. This can be explained by considering that an increment in the Yb^{3+} concentration leads to higher self-absorption of laser radiation around 1.07 μm, causing a drastic increment in the pump power at threshold, even preventing laser oscillation for higher-concentrated samples.[17] Stable laser generation was achieved with all the output mirrors used.

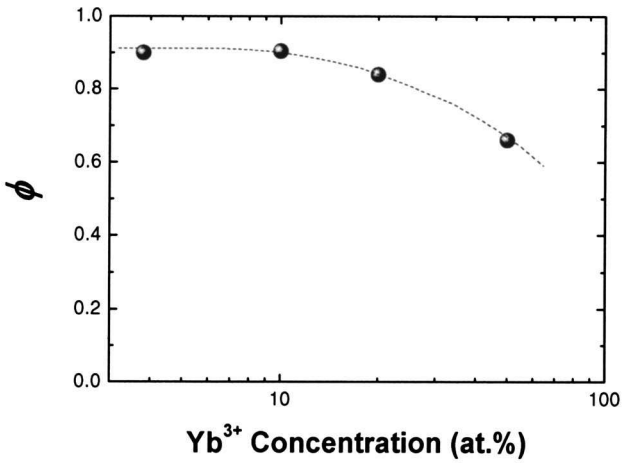

Fig. 7. Fluorescence quantum efficiency as a function of ytterbium concentration.

The spectral distribution for laser radiation was measured with a 0.01 nm resolution fiber-coupled spectrometer. The output laser power was monitored with a calibrated power meter. For thermal loading measurements a chromel alumel thermocouple was mechanically attached to the crystal so that its temperature was recorded. The crystal was thermally isolated by means of a teflon holder.

A. Thermal Loading Measurements

Figure 8(a) shows the steady increment in crystal temperature as a function of absorbed pump power when the Yb^{3+}:LuAG crystal was placed in the laser cavity with a 1% output coupler. Two different linear regimes with different slopes are clearly observed. The drastic change in ΔT_{st} versus P_{abs} takes place for an absorbed pump power of 0.8 W, this being the laser threshold observed for this output coupler transmittance [see Fig. 8(b), in which the laser curve is displayed]. This clearly indicates that the pump-induced thermal loading in the absence of stimulated emission is different from the pump-induced thermal loading in the presence of laser emission, as it has been already published regarding other Yb^{3+}-doped laser crystals.[24] Below threshold, the relationship between the increment in crystal temperature and the absorbed pump power is given by Eq. (5). In the presence of stimulated emission we can assume, in a first-order approximation, that all the electrons populating the lower-lying Stark component of the metastable state are de-excited by stimulated emission involving the emission of photons with a wavelength equal to the laser wavelength (λ_L = 1078 nm in the experimental conditions of Fig. 8). As a consequence the increment in crystal temperature will be given by[24]

$$\Delta T_{\mathrm{st}}^{la\ \sin g} = \alpha k 10^7 P_{\mathrm{abs}}\left(1 - \frac{\lambda_P}{\lambda_L}\right). \tag{6}$$

So that by comparing the slopes of the ΔT_{st} versus P_{abs} curves below and above laser threshold, the fluorescence quantum efficiency can be obtained from a combination of Eqs. (5) and (6).

After analyzing the data of Fig. 8, we have obtained a value of 0.82 for the fluorescence quantum efficiency. This value is reasonably close to the value obtained from the multiwavelength photothermal method described in Section 3 ($\phi \approx 0.88$) for this Yb^{3+} concentration, indicating the validity of these two methods to determine the fluorescence quantum efficiency. For the sake of comparison it should be noted that intracavity thermal loading measurements have been also used to determine the fluorescence quantum efficiency of other Yb^{3+}-doped laser crystals, such as Yb:YAB crystals.[24] In this case pump-induced thermal loading was measured by monitoring the thermal lensing of the gain medium, and the obtained value for the fluorescence quantum efficiency (0.88) was also close to unity. In the absence of concentration quenching, a high value for the fluorescence quantum efficiency in Yb^{3+}-doped crystals was in fact expected because of the large energy gap (around 11 000 cm^{-1}) between the excited and ground states. This large energy gap makes the number of phonons required for nonradiative de-excitation to be large and, therefore, the nonradiative probability to be small. The fact that quantum efficiency of Yb^{3+}:LuAG crystals remains close to unity for moderate doping levels makes this material interesting for high-power microchip lasers, since minimum thermal effects are expected in crystals showing appreciable absorption coefficients for pump radiation.

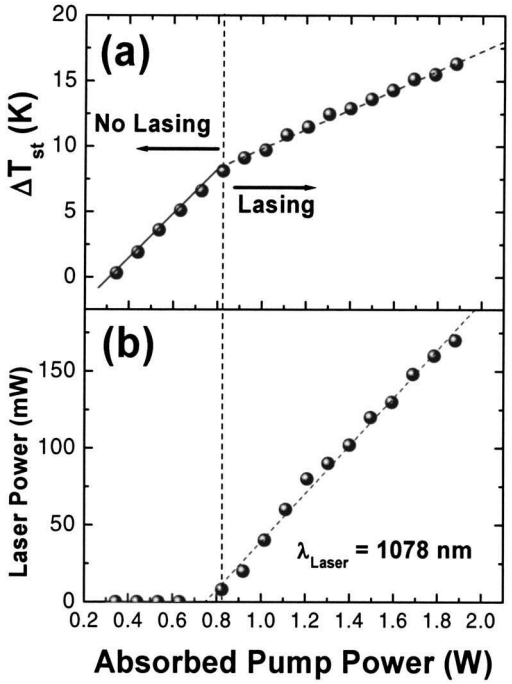

Fig. 8. (a) Steady increment in crystal temperature as a function of absorbed pump power obtained for a 12 at.% Yb^{3+}:LuAG laser crystal operating under diode pumping. (b) Laser power as a function of absorbed pump power obtained from a 12 at.% Yb^{3+}:LuAG laser crystal operating under diode pumping. Output mirror transmittance was 1 % in both cases.

B. Laser Output Tunability

One of the most interesting features of Yb^{3+}-doped materials is that they present broad emission and absorption bands owing to their characteristic strong electron–phonon coupling.[22] Broad absorption bands makes diode pumping easy, since a fine stabilization of diode temperature (diode wavelength) is not necessary. On the other hand, a broad emission band allows, in principle, a certain tunability in the laser wavelength by the inclusion of intracavity elements for wavelength selection. This possibility tunable laser light generation in the infrared is interesting for a variety of applications, including high-resolution spectroscopy. Furthermore, ultrashort pulse generation by mode locking requires that the laser gain extends over some wavelength range in such a way that the broader this range is the narrower the laser pulse that can be generated is.[25] In this sense the study of the tuning range of a given diode-pumped material could be used as an estimation of the propriety of this material for ultrashort pulse generation.

In this section we have studied the possibility of tunable laser light generation around 1.07 μm from a diode-pumped Yb:LuAG crystal. As in Section 4, we have used

the 12 at. % doped sample, but in this case the high-reflecting mirror was used in order to minimize the laser threshold. For wavelength selection a 2 mm tick birefringent filter (BF) was placed inside the cavity at Brewsted angle. Figure 9 shows the spectral distribution of laser radiation in the free-running mode (dashed curve) and when the birefringence filter was placed inside the cavity (solid curve). For these measurements the absorbed pump power was set to 1.8 W, and for the case of the spectrum corresponding to the free-running mode, it measured by averaging the signal for 1 min in order to minimize the effect of spectral instabilities. Owing to the broad emission band, the free-running spectrum has 3 nm FWHM. When the birefringence filter included in the cavity, wavelength selection takes place, and in this case FWHM is reduced down to 0.3 nm. It should be noted that the inclusion of the birefringence filter in the laser cavity leads to an increment in the intracavity losses and consequently to a decrease in the output laser power (from 40 mW down to 20 mW) Furthermore, by rotating the birefringence filter in its own plane, it was possible to tune the output laser wavelength from 1045 nm up to 1090 nm. Figure 10 shows the laser power as a function of the lasing wavelength for an absorbed pump power of 1.8 W. Stable laser radiation was obtained from 1045 nm up to 1095 nm, so that a total detuning range of 50 nm was obtained. This large detuning range is comparable with the detuning ranges obtained for other Yb^{3+}-doped laser crystals, such as Yb^{3+}:YAB,[26] and indicates a broad gain band, making Yb^{3+}:LuAG crystals possible candidates for ultrashort pulse generation.

5. CONCLUSION

We have grown high-quality LuAG:Yb^{3+} crystals of different concentrations with the vertical Bridgman method. With low-temperature spectroscopy the Stark sublevel structure of the $^2F_{7/2}$ ground state and the $^2F_{5/2}$ excited state has been determined. With room-temperature spectroscopy, the emission cross section was found to be higher than YAG:Yb^{3+}. The luminescence quantum efficiency was measured in samples with different Yb^{3+} concentrations; its value was found to be 90% for 10% Yb^{3+} and, generally speaking, reasonably high for concentrations well suited for laser diode pumping in end-pump configurations. The performance of the Yb:LuAG system as a tunable laser gain medium under 970 nm diode pumping has been also studied. In preliminary experiments we have obtained a total tuning range of 50 nm, this being comparable with the tuning ranges obtained for other Yb-doped laser materials. Owing to its good thermal conductivity, we can estimate that the LuAG:Yb^{3+} crystal is a promising laser crystal that could rival the most widely used YAG:Yb^{3+}.

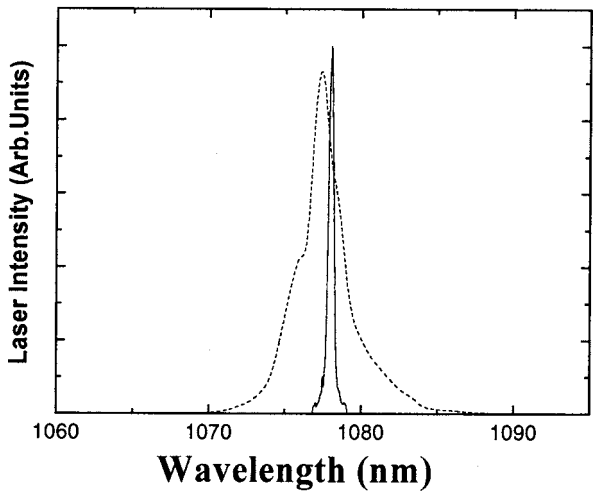

Fig. 9. Spectral distribution of laser radiation in the free-running mode (dashed curve) and when the birefringence filter was placed inside the cavity (solid curve). Data correspond to the 12 at.% doped sample.

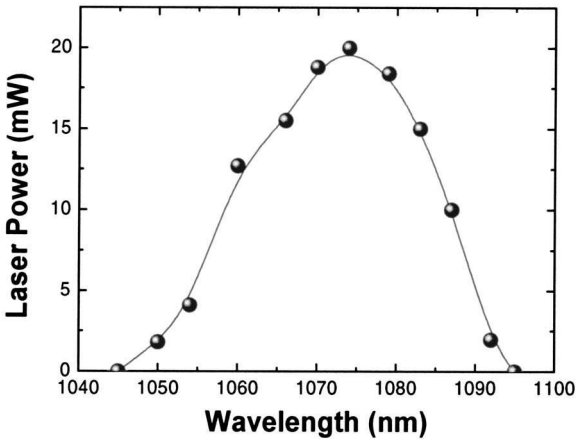

Fig. 10. Infrared laser power as a function of laser wavelength for an absorbed pump power of 1.8 W as obtained from the 12 at.% doped sample.

ACKNOWLEDGMENTS

This work was supported by the Comunidad Autónoma de Madrid (CAM) under Projects 07N/0020/2002 and GR/MAT/0110/2004 and by the Comisión Interministerial de Ciencia y Tecnología (CICYT) under project MAT2001-0167. D. Jaque thanks the Ministerio de Ciencia y Tecnologia of Spain for a Ramon y Cajal contract.

REFERENCES

1. Kh. S. Bagdasarov, G. A. Bogomolova, D. N. Vilegzhanin, A. A. Kaminskii, A. M. Kevorkov, A. G. Petrosyan, and A. M. Prokhorov, "Luminescence and stimulated emission of Yb3+ ions in aluminum garnets," Dokl. Akad. Nauk SSSR **216**, 1247–1249 (1974).
2. D. S. Sumida, T. Y. Fan, and R. Hutcheson, "Spectroscopy and diode-pumped lasing of Yb^{3+} doped $Lu_3Al_5O_{12}$(Yb:LuAG)," in *Advanced Solid-State Lasers*, B. H. T. Chai and S. A. Payne, eds. (Optical Society of America, 1995), Vol. 24, pp. 348–350.
3. T. Kasamatsu, H. Sekita, and Y. Kuwano, "Temperature dependence and optimization of 970-nm diode-pumped Yb:YAG and Yb:LuAG lasers," Appl. Opt. **38**, 5149–5153 (1999).
4. F. Euler and I. A. Bruce, "Oxygen coordinates of compounds with garnet structure," Acta Crystallogr. **19**, 971–974 (1965).
5. A. G. Petrosyan and G. O. Shirinyan, "Peculiarities in crystallization of rare-earth aluminum garnets from non-stoichiometric melts," Inorg. Mater. **29**, 258–261 (1993).

6. K. L. Ovanesyan, A. G. Petrosyan, G. O. Shirinyan, and A. A. Avetisyan, "Optical dispersion and thermal expansion of Lu3Al5O12, Er3Al5O12 and Y3Al5O12 garnets," Inorg. Mater. **3**, 459–462 (1981).
7. S. Chenais, F. Druon, F. Balembois, P. Georges, A. Brenier, and G. Boulon, "Diode-pumped Yb:GGG laser: comparison with Yb:YAG," Opt. Mater. **22**, 99–106 (2003).
8. G. A. Slack and D. W. Oliver, "Thermal conductivity of garnets and phonon scattering by rare-earth ions," Phys. Rev. B **4**, 592–609 (1971).
9. A. G. Petrosyan, "Crystal growth of laser oxides in the vertical Bridgman configuration," J. Cryst. Growth **139**, 372–392 (1994).
10. T. I. Butaeva, A. G. Petrosyan, and A. K. Petrosyan, "Optical centers of europium and ytterbium ions in aluminum garnets," Inorg. Mater. **2**, 430–434 (1988).
11. F. D. Patel, E. C. Honea, J. Speth, S. A. Payne, R. Hutcheson, and R. Equall. "Laser demonstration of Yb3Al5O12 (YbAG) and materials properties of highly doped Yb : YAG," IEEE J. Quantum Electron. **37**, 135–144 (2001).
12. F. Auzel, F. Bonfigli, S. Gagliari, and G. Baldaccnini, "The interplay of self-trapping and self-quenching for resonant transitions in solids; role of a cavity," J. Lumin. **94–95**, 293–297 (2001).
13. A. Yoshikawa, G. Boulon, L. Laversenne, H. Canibano, K. Lebbou, A. Collombet, Y. Guyot, and T. Fukuda, "Growth and spectroscopic analysis of Yb^{3+}-doped $Y_3Al_5O_{12}$ fiber single crystals," J. Appl. Phys. **94**, 5479–5488 (2003).
14. Y. Guyot, H. Canibano, C. Goutaudier, A. Novoselov, A. Yoshikawa, T. Fukuda, and G. Boulon, "Yb^{3+}-doped $Gd_3Ga_5O_{12}$ garnet single crystals grown by the micro-pulling down technique for laser application. Part I: Spectroscopic properties and assignment of energy levels," Opt. Mater. **27**, 1658–1663 (2005).
15. Y. Guyot, H. Canibano, C. Goutaudier, A. Novoselov, A. Yoshikawa, T. Fukuda, and G. Boulon, "Yb^{3+}-doped $Gd_3Ga_5O_{12}$ garnet single crystals grown by the micro-pulling down technique for laser application. Part 2: Concentration quenching analysis and laser optimization," Opt. Mater. **28**, 1–8 (2006).
16. A. A. Kaminskii *Laser Crystals* (Springer, 1981).
17. W. P. Risk. "Modeling of longitudinally pumped solid-state lasers exhibiting reabsorption losses," J. Opt. Soc. Am. B **5**, 1412–1423 (1988).
18. P. Wang, J. M. Dawes, P. Dekker, and J. A. Piper. "Highly efficient diode-pumped ytterbium-doped yttrium aluminum berate laser," Opt. Commun. **174**, 467–470 (2000).
19. D. Jaque and J. Gracía Solé, "Temperature decrease induced by stimulated emission in the Nd3+ ion-doped $YAl_3(BO_3)_4$ crystal," Chem. Phys. Lett. **334**, 309–313 (2001).
20. J. A. Muñoz, J. O. Tocho, and F. Cussó, "Photoacoustic determination of the luminescent quantum efficiency of Yb3+ ions in lithium niobate," Appl. Opt. **37**, 7096–7099 (1998).
21. S. M. Lima, A. S. S. de Camargo, L. A. O. Nunes, and T. Catunda. "Fluorescence quantum efficiency measurements of excitation and nonradiative deexcitation processes of rare earth 4*f*-states in chalcogenide glasses," Appl. Phys. Lett. **81**, 589–591 (2002).
22. B. Henderson and G. F. Imbusch, *Optical Spectroscopy of Inorganic Solids* (Clarendon, 1989).
23. D. Jaque, Z. D. Luo, and J. García Solé. "Quantum efficiency of Nd-doped lasers measured by pump-induced crystal heating: application to the Nd3+:Gd-2(MoO4)(3) crystal," Appl. Phys. B **72**, 811–814 (2001).
24. J. L. Blows, P. Dekker, P. Wang, J. M. Dawes, and T. Omatsu, "Thermal lensing measurements and thermal conductivity of Yb : YAB," Appl. Phys. B **76**, 289–292 (2003).
25. W. Koechner, *Solid-State Laser Engineering*, 5th ed. (Springer-Verlag, 1999).
26. P. Wang, P. Dekker, J. M. Dawes, J. A. Piper, Y. Liu, and J. Wang. "Efficient continuous-wave self-frequency-doubling green diode-pumped Yb:YA13(BO3)(4) lasers," Opt. Lett. **25**, 731–733 (2000).